LARGE DYNAMIC RANGE ATOMIC FORCE MICROSCOPE

In semiconductor manufacturing, the shrink following Moore's law requires ever tighter overlay and registration between the different (material) layers. For accurately characterising this overlay and registration, TNO has developed a large dynamic range atomic force microscope demonstrator; the LDR-AFM can measure marker-to-feature distances over several millimeters with sub-nanometer reproducibility. It features a highly stable metrology concept and a 6-degrees-of-freedom positioning platform (hexapod) carrying an AFM scan head able to move the AFM probe tip. Repeatability measurements have demonstrated that both drift and reproducibility figures are well below the smallest feature size of the newest semiconductor processing nodes.

RODOLF HERFST, MAARTEN VAN ES, STEFAN KUIPER, GERT WITVOET, JOOST PETERS AND ROB WILLEKERS

Introduction

Scanning probe microscopy (SPM) is a form of microscopy that uses a probe to scan a surface in order to form high-resolution images far below the diffraction limit of light in the visible range. Various types and implementations have been developed over the year, but atomic force microscopy (AFM) in particular has revolutionised the imaging industry. It was invented in 1986 [1] and offers high-resolution (down to atomic scale [2]) imaging on relatively cheap and simple instruments.

Two significant drawbacks of the technique however are that it is relatively slow (a few minutes or more for a single high-resolution image), and capable of imaging on only relatively small length scales (typically 100 micron or less [3]). As a consequence, AFM has been mostly restricted to research and laboratory settings and its strengths have not been widely applied in production environments, although there are some examples where it has been used in semiconductor fabs for inspection and process control purposes [4-5].

Naturally, the unique strong points of AFM have led to efforts to mitigate its drawbacks for both general-purpose imaging as well as metrology purposes. Examples are the development of video-rate AFM [6], the high-throughput parallel AFM developed at the Netherlands Organisation for Applied Scientific Research (TNO), now being commercialised by Nearfield Instruments [7], and the large dynamic range AFM (LDR-AFM) [8-10]. This last one aims to drastically increase the length scale accessible by the technique and is the topic of this article. It combines an AFM measurement head optimised for sub-nm accuracy with a highly accurate long-stroke motion stage with six degrees of freedom (6-DoF). This is then mounted in a metrology frame large enough to accommodate 300-mm wafers. We will present an overview of the system's concept and implementation, as well as experimental results that showcase the high performance achieved.

The tool is aimed at providing sub-nm metrology over a distance of several millimeters (i.e., dynamic range > 10^6). This can be used to characterise both overlay (relative shift) and registration (absolute shift, with respect to a coordinate system) between the different (material) layers in chip fabrication. In established overlay metrology tools, alignment markers are used to assess how large the relative shift between two or more layers is. If the markers are then correctly printed with respect to each other, it is assumed that the device features printed in the same exposure steps as the alignment markers are also placed correctly with respect to each other. However, this is not necessarily the case, especially for the extremely small device features that are possible with the newest lithography techniques, such as EUV. For example, features with a very small pitch can be affected differently by lithography lens aberrations than the coarser marker shapes that are printed for alignment.

To accurately determine overlay of device features associated with, e.g., two different lithography steps, the LDR-AFM is used twice to very accurately measure the distance between a device feature and an overlay marker in each of the two layers. After this, a more traditional (optical) overlay metrology tool determines overlay between the two marker structures. This then gives enough information to infer the overlay between the device features, even if one of those features is not visible anymore in, e.g., a SEM (scanning electron microscope) or AFM image. Apart from aiding in overlay and registration, the LDR-AFM can

AUTHORS' NOTE

Rodolf Herfst (research scientist), Maarten van Es (scientist), Stefan Kuiper (mechatronics system engineer), Gert Witvoet (dynamics and control specialist), Joost Peters (junior control engineer) and Rob Willekers (research manager, department head) are all associated with the OptoMechatronics department of TNO Technical Sciences in Delft (NL).

rodolf.herfst@tno.nl
www.tno.nl

be used to obtain detailed profile information of both device and marker features.
In the next sections, we will first discuss the LDR-AFM's hardware, followed by a brief explanation of how the hexapod positioner is controlled and deals with the inherent cross-couplings. Then, we will go into how the AFM control loop functions. Finally, we will show some results obtained with the system that highlights its potential for metrology applications

Hardware details

A schematic overview of the system is shown in Figure 1a. At the heart of it, the AFM head with a tilted probe is situated (Figures 1b and 1c). A 6-DoF hexapod positioner [11] can move the AFM head within a hexagon-shaped box (8 mm diameter and 4 mm height). The hexapod is attached to a metrology frame in which a 300-mm wafer can be mounted. The metrology frame is attached to a force frame through (secondary) dampers, which are connected to the ground through the primary dampers.

The 6-DoF hexapod positioner uses six voice-coil actuators via flexural hinges to realise translation and rotation. Of course, if no current is flowing through the coils, no (magnetic) forces are generated by them. Therefore, counteracting gravity forces using only voice coils would lead to a large power dissipation, which would in turn heat up the voice coils. In order to reduce this, gravity forces are compensated by magnets on each of the three corners of the stage (see Figure 1b). These magnets are positioned between sets of external magnets, resulting in an upward force on the stage.

To determine the position and rotation of the hexapod, six laser interferometers are incorporated. The interferometer beams are pointed at target mirrors on each side of the stage. When the hexapod is controlled, the point of which the position should be most accurately known is the tip of the cantilever. In order to reduce Abbe errors at this point, the interferometers are in an orthogonal configuration and the normal of each mirror points toward the AFM probe.

In the AFM head (Figure 2), the AFM chip is attached to the probe holder, underneath which a dither piezo is situated that excites the cantilever. Cantilever motion is measured using the optical beam deflection technique (OBD), featuring a laser diode, a focussing lens, a quadrant cell and associated electronics. The AFM head is held in position in the central hole of the hexapod positioner using dowels and magnetics and can easily be removed for exchanging the cantilever.

Note that the AFM head by design does not have a separate (fast) *z*-stage for the AFM chip, which is common in general-purpose AFMs, but is not required in this specific application, for which a slower, more accurate *z*-stage suffices. Typical piezo actuators used for this purpose (i.e. a separate *z*-stage) are subject to creep and hysteresis,

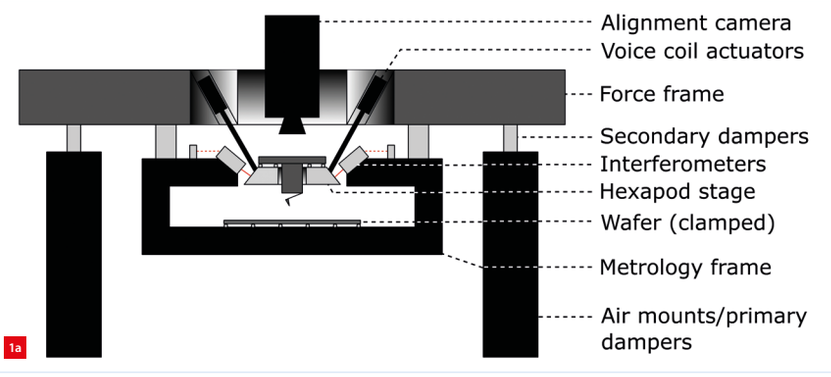

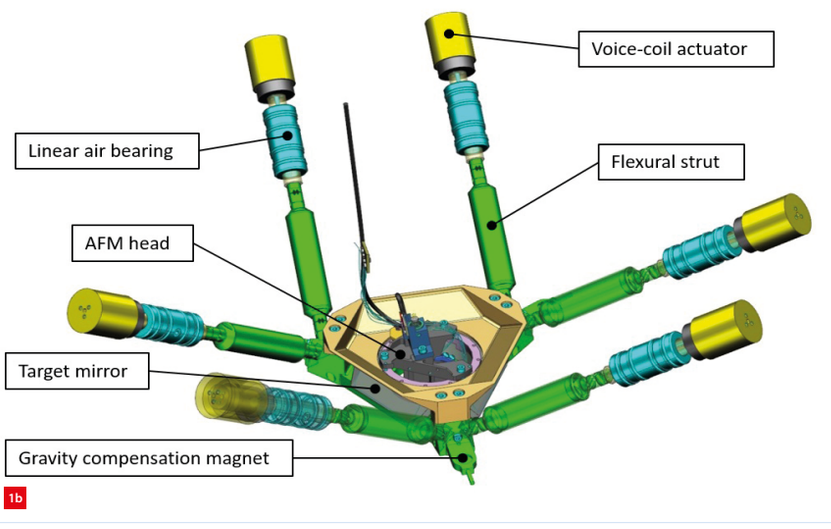

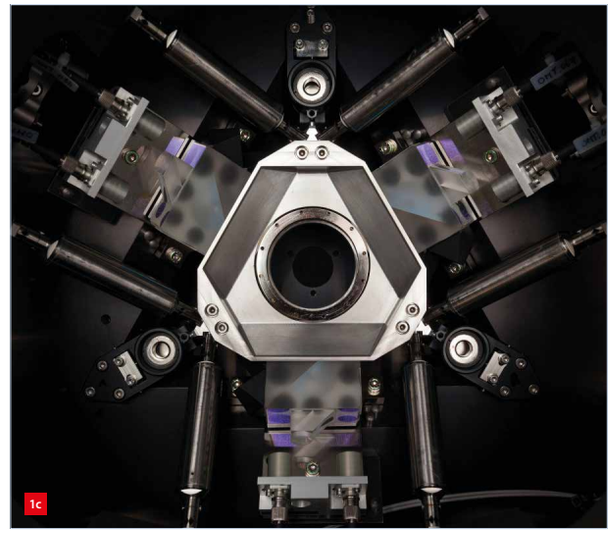

The large dynamic range AFM system.
(a) Concept.
(b) Design (CAD drawing)
(c) Realisation with the hexapod 6-DoF positioner and mounted AFM head.

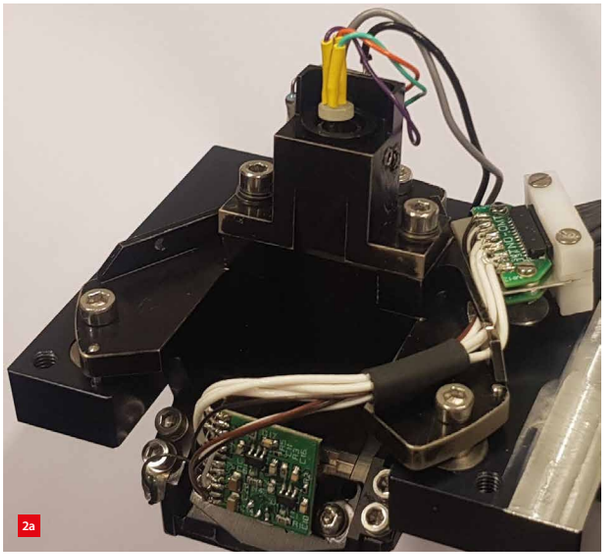

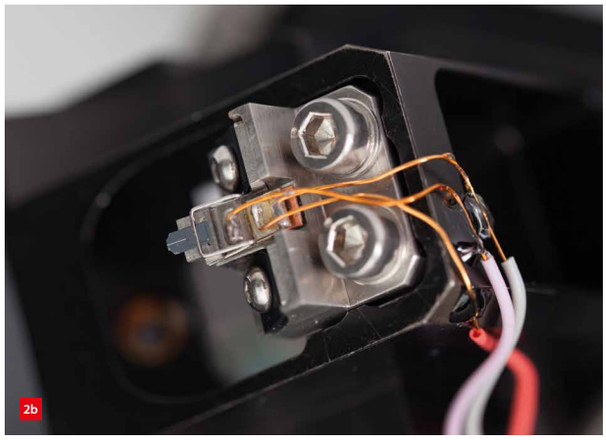

Unmounted AFM head.
(a) Showing laser connection wires (top, white socket with yellow shrink tube) and quadrant cell electronics (bottom, green PCB).
(b) Close-up of the cantilever holder with the AFM chip mounted (obscured by the quadrant cell).

negatively affecting the accuracy of the AFM measurement as the extension of such a piezo actuator would not be captured adequately by the interferometers. This is due to the fact that they measure the position of the stage as a whole, i.e. not directly the location of the AFM cantilever.

Hexapod control

While the described hexapod positioner concept has a number of advantages over alternatives such as a spindle-based approach, including very low hysteresis, no slip-stick effects and fast actuation, it does need active feedback control to be operated. Although the six actuators and six interferometers are sufficient to actuate and measure all three displacement axes and three rotation axes, the actuation and sensing axes are (by design) obviously not orthogonal. Hence, to control this cross-coupled platform, the multiple-in-multiple-out (MIMO) control scheme as shown in Figure 3 has been implemented. This approach decouples the problem into six independent single-in-single-out (SISO) control loops. Matrices transform the signals in the control loop between three different coordinate systems:

1. Rigid-body motion space (orthogonal, indicated in black, origin of coordinates at cantilever).
2. Actuator sensor space (indicated in blue).
3. Controller space (indicated in red, origin of coordinates at centre of gravity).

Matrices T_u and T_y transform the system's transfer function $H(s)$ into rigid-body coordinates, allowing the user to define setpoints in terms of translations and rotations of the AFM cantilever. Moreover, V_u and V_y further optimise the decoupling for controller design (by shifting the coordinate system origin to the hexapod's centre of gravity), so as to minimise the remaining interaction around the targeted bandwidth and to allow for the usage of six SISO controllers.

The initial design of the decoupling matrices and the SISO controllers was fully based on predictive models [3]. Because we use a static magnetic gravity-compensation scheme, the hexapod stage is open-loop unstable. In order to be able to stabilise the stage on first use, a decently fast initial controller was required. This was constructed using a finite-element model (FEM) of the stage, which resulted in an initial open-loop bandwidth of about 100 Hz. Having this as a starting point, the six controllers were further optimised, yielding a bandwidth of 210 Hz in x- and y-direction, and 270 Hz in z-direction [12]. Although this latter bandwidth is rather low for topography tracking in a regular AFM, it is sufficiently high for the distance measurements that this tool is designed for: a measurement cycle of about one minute is enough for sub-nm reproducibility. In the experimental results section, we will show measurement data corroborating this claim.

AFM control

In addition to the controller required to operate the positioning stage, another loop is necessary to perform actual AFM measurements with it. A (simplified) schematic

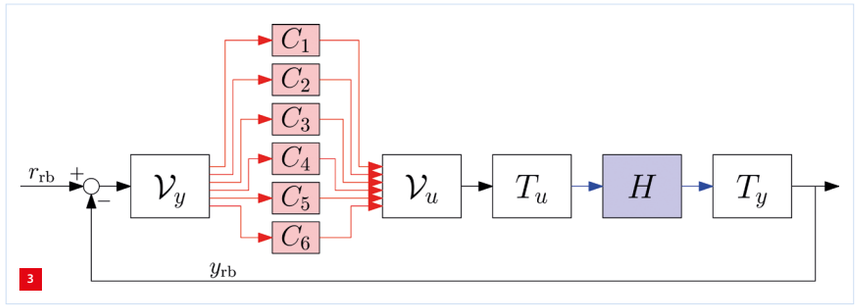

Implemented 6-DoF control scheme with decoupling matrices; the matrices T_u and T_y transform the system H into rigid-body coordinates, whereas V_u and V_y further decouple the system to allow for the usage of six SISO controllers.

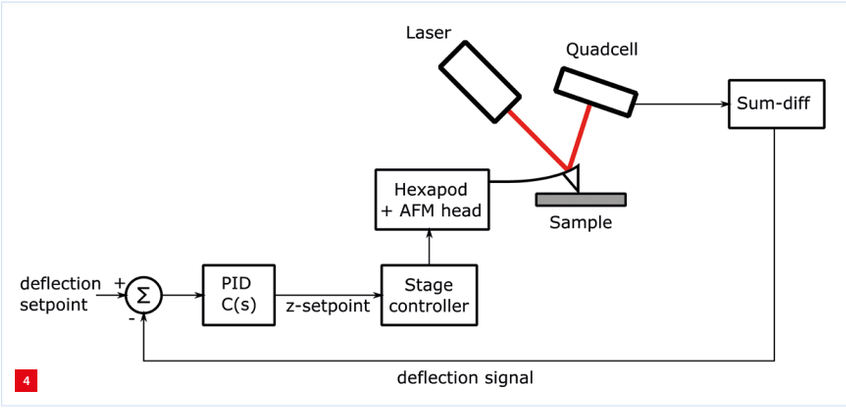

Control loop for contact-mode AFM. PID adjusts the z-setpoint of the positioning stage controller executing the control loop of Figure 3.

of this is shown in Figure 4. This shows a cantilever in contact with a sample, which causes the cantilever to bend. The laser, quadrant detector, and sum-difference amplifier together perform the OBD sensing and generate a signal proportional to the bending of the cantilever (deflection signal). The AFM control loop keeps the deflection equal to the deflection setpoint by continuously adjusting the z-setpoint of the positioning stage.

Apart from the contact-mode AFM shown here, tapping-mode AFM has been implemented as well. For this, the cantilever is excited at its resonance, and instead of acting on the deflection, the control loop adjusts its height to keep the resulting cantilever vibration amplitude constant. This mode can greatly reduce both tip- and sample-wear compared to the contact mode.

Experimental results

After the LDR-AFM was built and control was implemented and optimised, we performed a series of tests to characterise the performance of the full system. Since the system is a metrology tool, two very important performance metrics are the system's noise and reproducibility. To assess the positioning noise of the stage, the closed-loop interferometer signals have been traced for two minutes and converted to rigid-body motion of the stage. From this data, the power spectral density graph as shown in Figure 5a was determined. The cumulative amplitude spectrum in Figure 5b shows the overall rms noise is below 0.7 nm and 0.4 nm in *xy* and *z*, respectively (note that the true stage noise will be slightly lower, as high-frequent sensor noise will not propagate into stage motion). This is low enough to accurately resolve nm-scale structures, and allows for distance measurements with sub-nm resolution.

The problem with Figure 5 is that it does not necessarily say anything about the actual stage motion, it is simply how the feedback sensor measures it; hence one still needs to validate this metrology by some absolute validation sensor or measurement.

While the above results show that the contribution of the tracking error to overall measurement reproducibility is low, this does not necessarily mean we can conclude that likewise the actual stage motion reproducibility is good; the graphs are simply based on what the sensors report as stage motion. Hence, for real certainty one still needs to validate this metrology by some absolute validation sensor or measurement. To get such an absolute validation, an end-to-end drift measurement was performed. A cantilever was loaded on the AFM head, and the contact-mode AFM control loop was activated while the *xy*-position was kept stationary. The AFM control loop then kept the stage in close proximity to a flat sample by making sure the cantilever deflection remains constant. While in this state, the interferometer-derived *z*-signal was measured for more than 5 hours, the result of which is shown in Figure 6. As can be seen, the system exhibited less than 20 nm drift over the full duration of the measurement, i.e. under 50 pm/minute.

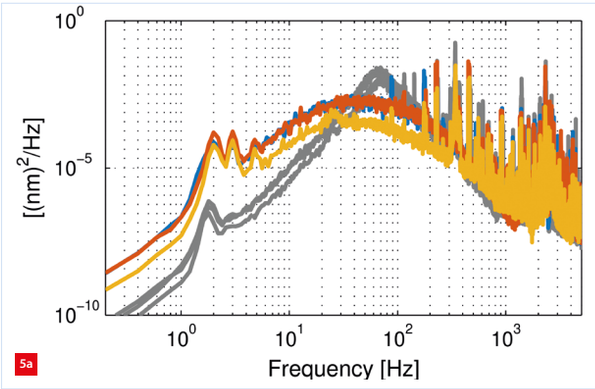

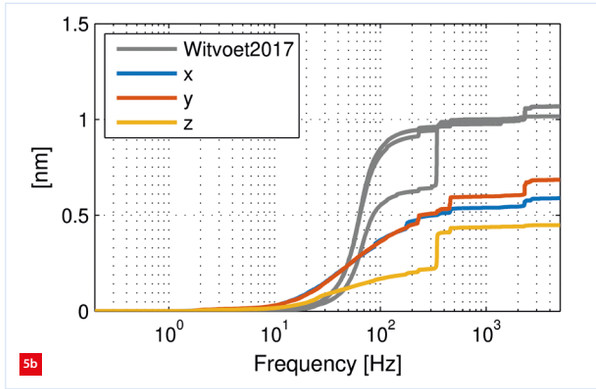

Closed-loop error in translational directions at a certain stand-still position.
Grey lines: preliminary controller.
Coloured lines: optimised controller.
(a) Power spectral density.
(b) Cumulative amplitude spectrum (Witvoet2017 = [10]).

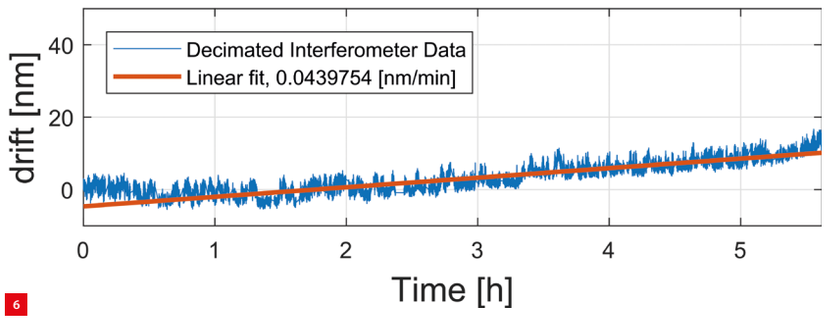

Drift measurement of the stage z-position, while controlling both its x- and y-position and the cantilever direction to constant values. Over several hours an average z-motion of less than 50 pm/min is observed, while the 1-minute moving average varies only a few nm. Data is shown decimated by a factor 100 with respect to the real-time control system's sampling rate.

Table 1
Summary of the LDR-AFM system performance. Value for $\sigma(d_{1,2})$ (i.e., the rms variation in the length measurements) obtained from data points in the flat section in Figure 8 (i.e., after 5 hours).

Performance variable	Value	Unit
Stage bandwidth, *x, y*	210	Hz
Stage bandwidth, *z*	270	Hz
x, y stand-still servo error	< 0.7	nm rms
z stand-still servo error	< 0.4	nm rms
ϕ, θ, ψ stand-still servo error	< 15	nrad rms
Stand-still drift in *z*	< 50	pm/min
Distance drift in *x*, > 1 mm stroke	< 20	pm/min
$\sigma(d_{1,2})$ over > 1 mm stroke, 12 hr	< 0.25	nm

To determine the stability in lateral (*xy*) direction, a more complicated kind of test is required, which resembles real-world overlay and registration tests more closely, as schematically illustrated in Figure 7. A sample with SRAM (static random-access memory) cells is loaded into the system, and the AFM control loop is configured and activated. Two SRAM cells that are nominally 1.3 mm apart are measured, and the position of the left sidewall of each of the two SRAM cells is identified. Then, a distance measurement loop is set up that repeatedly performs the following steps:

1. Measure sidewall on SRAM cell 1.
2. Retract stage.
3. Move to SRAM cell 2.
4. Approach sample.
5. Measure sidewall on SRAM cell 2.
6. Retract stage.
7. Move back to SRAM cell 1.

Each distance measurement cycle took approximately one minute. In post-processing, for each sidewall measurement the lateral position of the sidewall was extracted. From this we calculated the distance in two slightly different ways:

- Feature 2 measured after feature 1; $D_1(n) = x_2(n) - x_1(n)$.
- Feature 2 measured before feature 1; $D_2(n) = x_2(n) - x_1(n+1)$.

This way, if the positions of the features have a common lateral drift component, its effect will show up as a difference between $D_1(n)$ and $D_2(n)$. To further improve the distance measurement, a moving average using four consecutive cycles is applied to the data set; $D'_1(n) = ¼ \Sigma_{i=0..3} D_1(n-i)$. This effectively makes the test time for a single point four minutes.

As can be seen in the result (Figure 8), no significant effect of common lateral shifting is visible; the red and blue markers follow the same trends and do not significantly separate. As for the reproducibility, during the first 4-5 hours of the test, there was about 1.5 nm change in the 1.3 mm distance measurement (< 20 pm/minute). After 5 hours the trend became flat (we expect the system was thermally stabilised), and the obtained length values exhibited < 0.25 nm rms variation. A summary of the test results in shown in Table 1.

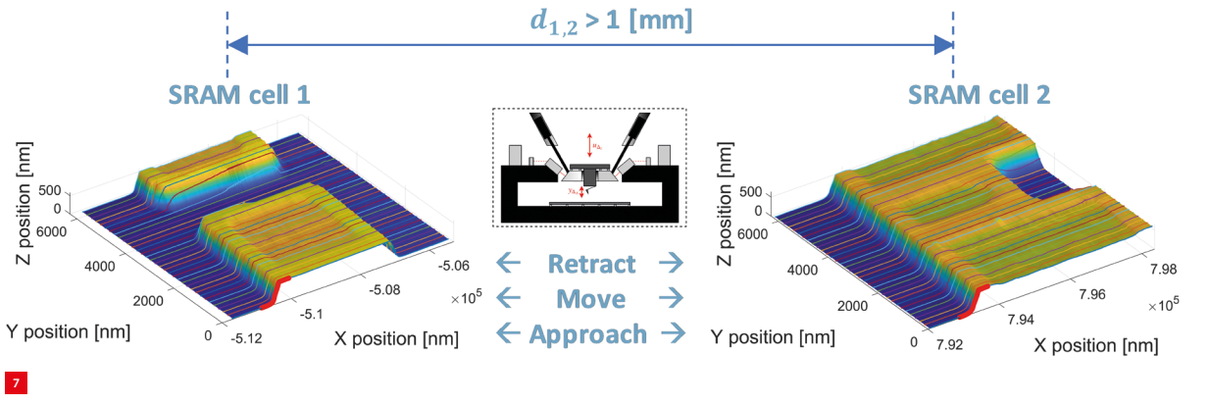

Schematic illustration of a distance measurement cycle: 3D images of actual data obtained with the LDR-AFM; in red the portion of the edge that is remeasured in each distance measurement cycle.

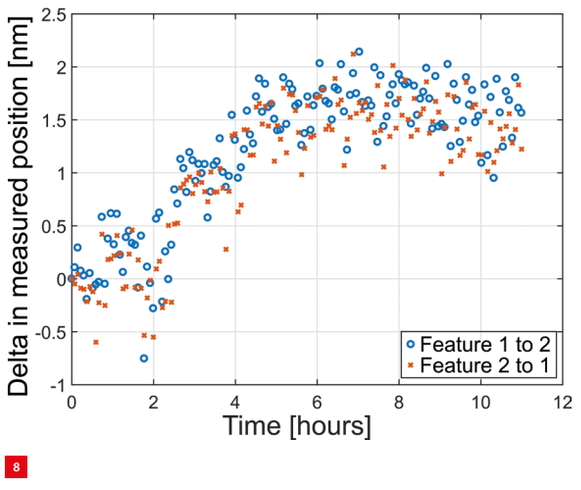

Change in measured feature distance as function of time. Each data point represents the average of four distance measurement cycles.

Summary and conclusion

In this article, the design and first results of the LDR-AFM developed by TNO have been presented. A high-performance instrument was realised using a unique combination of a large-range positioning stage (Figure 9) with full 6-DoF control, accurate metrology, separation of force and metrology frames, and a very sensitive AFM sensing head. The results show the predictability and reproducibility of the LDR-AFM and demonstrate its potential for sub-nm metrology over several millimeters distance. Future work includes further optimising the metrology tool's environmental conditions, investigating metrology applications for the tool, and addressing metrology-specific challenges and measurement recipe development.

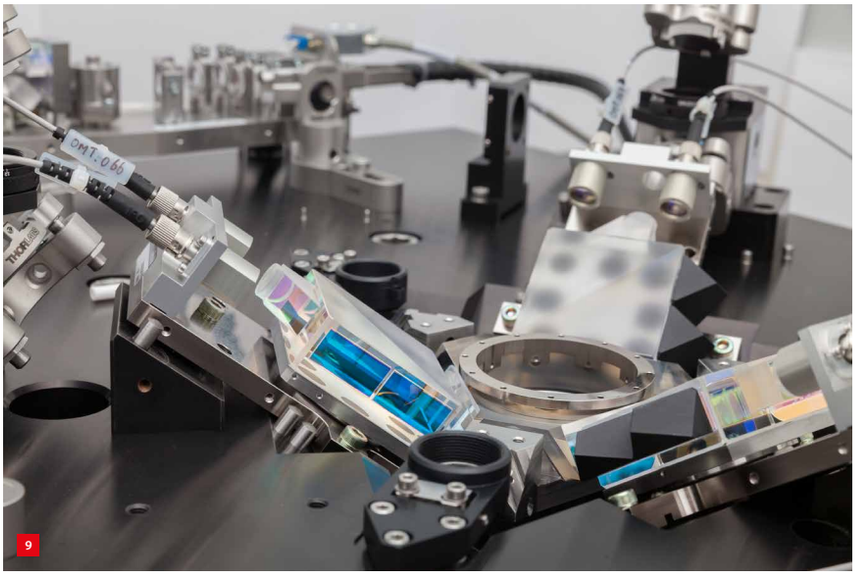

Close-up of the LDR-AFM's positioning stage. Right of centre is the hexapod positioning stage with a hole for accommodating the AFM head. Also visible are the laser interferometers consisting of fibres with collimation optics (top-left, top-right), beam-splitters (large glass blocks with blue-coloured rectangles due to a reflective dielectric coating on two of the mirrors), and mirrors attached to the positioning stage. (Photo: Henri Werij)

Acknowledgments

The authors would like to thank the other project members at TNO for their vital contributions to the realisation of the LDR-AFM, and ASML for their valuable inputs. Furthermore, we would like to thank prof.dr. H.G.C. Werij for his photo (Figure 9) of the LDR-AFM's positioning stage, featured on the cover of this Mikroniek issue.

REFERENCES

[1] C. Werner, P.C.J.N. Rosielle, and M. Steinbuch, "Design of a long stroke translation stage for AFM", *Int. J. Mach. Tools Manuf.*, 50(2), pp. 183-190, 2010.
[2] F. Ohnesorge, "True atomic resolution by atomic force microscopy through repulsive and attractive forces", *Science*, 260 (5113), pp. 1451-1456, 1993.
[3] P. Eaton, and P. West, *Atomic Force Microscopy*, Oxford University Press, New York, NY, USA, 2010.
[4] H.U. Danzebrink, et al., "Advances in scanning force microscopy for dimensional metrology", *CIRP Annals - Manufacturing Technology*, 55(2), pp. 841-878, 2006.
[5] J. Foucher, R. Thérèse, Y. Lee, S.-I. Park, and S.-J. Cho, "Introduction of next-generation 3D AFM for advanced process control", *Proc. SPIE*, vol. 8681, p. 868106, 2013.
[6] G. Schitter, and M.J. Rost, "Scanning probe microscopy at video-rate", *Materials Today*, 11 (special issue), pp. 40-48, 2008.
[7] H. Sadeghian, et al., "High-throughput atomic force microscopes operating in parallel", *Review of Scientific Instruments*, 88, p. 033703, 2017.
[8] S. Kuiper, E. Fritz, and W. Crowcombe, et al., "Large dynamic range atomic force microscope for overlay improvements", *Proc. SPIE*, vol. 9778, p. 97781B, 2016.
[9] G. Witvoet, et al., "First results from the Large Dynamic Range Atomic Force Microscope for overlay metrology", *Proc. SPIE*, vol. 10959, *doi: 10.1117/12.2514044*, 2019.
[10] G. Witvoet, et al., "Predictive-model-based MIMO motion control of an unstable 6-DoF hexapod stage for overlay measurements", *Proc. Conf. Control Technol. Appl.*, pp. 726-731, 2017.
[11] D. Stewart, "A platform with six degrees of freedom", *Proc. Inst. Mech. Eng.*, 180 (1), pp. 371-386, 1965.
[12] G. Witvoet, et al., "Line-to-line repetitive control of a 6-DoF hexapod stage for overlay measurements using Atomic Force Microscopy", *Proc. American Control Conference 2019*, pp. 2464-2469, 2019.